How to cite: *Angew. Chem. Int. Ed.* **2022,** *61,* e202202182
International Edition: doi.org/10.1002/anie.202202182
German Edition: doi.org/10.1002/ange.202202182

Na^+ Conductivity

Directed Dehydration as Synthetic Tool for Generation of a New Na_4SnS_4 Polymorph: Crystal Structure, Na^+ Conductivity, and Influence of Sb-Substitution

Felix Hartmann, Assma Benkada, Sylvio Indris, Michael Poschmann, Henning Lühmann, Patrick Duchstein, Dirk Zahn, and Wolfgang Bensch**

Abstract: We present the convenient synthesis and characterization of the new ternary thiostannate Na_4SnS_4 (space group $I4_1/acd$) by directed removal of crystal water molecules from $Na_4SnS_4{\cdot}14\,H_2O$. The compound represents a new kinetically stable polymorph of Na_4SnS_4, which is transformed into the known, thermodynamically stable form (space group $P\bar{4}2_1c$) at elevated temperatures. Thermal co-decomposition of mixtures with $Na_3SbS_4{\cdot}9\,H_2O$ generates solid solution products $Na_{4-x}Sn_{1-x}Sb_xS_4$ ($x = 0.01$, 0.10) isostructural to the new polymorph ($x = 0$). Incorporation of Sb^{5+} affects the bonding and local structural situation noticeably evidenced by X-ray diffraction, ^{119}Sn and ^{23}Na NMR, and ^{119}Sn Mössbauer spectroscopy. Electrochemical impedance spectroscopy demonstrates an enormous improvement of the ionic conductivity with increasing Sb content for the solid solution ($\sigma_{25°C} = 2\times10^{-3}$, 2×10^{-2}, and 0.1 mS cm^{-1} for $x = 0$, 0.01, and 0.10), being several orders of magnitude higher than for the known Na_4SnS_4 polymorph.

[*] F. Hartmann, A. Benkada, H. Lühmann, W. Bensch
Institute of Inorganic Chemistry
Christian-Albrecht University of Kiel
Max-Eyth-Str. 2, 24118 Kiel (Germany)
E-mail: fhartmann@ac.uni-kiel.de
wbensch@ac.uni-kiel.de

S. Indris
Institute of Applied Materials, Karlsruhe Institute of Technology
Hermann-von-Helmholtz-Platz 1
76344 Eggenstein-Leopoldshafen (Germany)

M. Poschmann
Max-Planck-Institute for Chemical Energy Conversion
Stiftstr. 34–36, 45470 Mülheim an der Ruhr (Germany)

P. Duchstein, D. Zahn
Computer Chemistry Center
Friedrich-Alexander-Universität Erlangen-Nürnberg
Nägelsbachstr. 26, 91052 Erlangen (Germany)

Introduction

The structures of thiostannate compounds include different anionic units like $[SnS_4]^{4-}$, $[Sn_2S_6]^{4-}$, $[Sn_2S_5]^{2-}$, $[Sn_2S_7]^{6-}$, $[Sn_2S_8]^{2-}$, $[Sn_3S_7]^{2-}$, $[Sn_3S_8]^{4-}$, $[Sn_4S_{10}]^{4-}$ or $[Sn_5S_{12}]^{4-}$, which are charge compensated by metal cations.[1–9] The structural versatility of thiostannate anions is due to the variable coordination number as well as the variable oxidation state of Sn. In the above-mentioned thiostannate anions Sn exhibits the coordination number 4 (tetrahedron), 5 (trigonal bipyramid), or 6 (octahedron). In addition, Sn occurs mainly in the oxidation state IV, but compounds with different oxidation states like II/IV or III/IV were also reported.[10–12] Thiostannates with metal cations as counter ions were mainly synthesized using the molten-flux approach,[13,14] or via high-temperature syntheses.[15–19] Thiostannates with protonated amine molecules, transition metal cations, or transition metal complexes as counter ions compensating the negative charge of the $[Sn_xS_y]^{n-}$ anions were mostly prepared under solvothermal conditions.[9,20–35] Applying suitable precursors, the preparation of thiostannates at room temperature was also reported.[36–41] These examples demonstrate the broad variety of synthetic approaches established in the thiostannate chemistry.

Motivated by the intense research in the field of all-solid-state batteries (ASSBs), where sulfidic compounds came into the focus including thiophosphates,[42–49] or thioantimonate based solid electrolytes,[50–62] we searched for possible solid-state electrolytes (SSEs) on the basis of chalcogeniodostannates. Indeed, first steps in this direction were reported for Li^+ SSEs: Li^+ ion conducting thio- and selenostannates were prepared by a high-temperature route combined with extraction or thermal evaporation ($T =$ 320 °C) methods of intermediately synthesized solvates.[63,64] More recently, mixed quaternary Na^+ superionic conductors based on the thiostannate chemistry were discovered, e.g., the series of compounds $Na_{4-x}Sn_{1-x}Sb_xS_4$[50,56] and $Na_{11}Sn_2PS_{12}$[47–50] show promising room temperature Na^+ ion conductivities >0.5 mS cm^{-1}. Moreover, excellent cycling and rate stabilities were observed using $Na_{3.75}Sn_{0.75}Sb_{0.25}S_4$ or $Na_{10.8}Sn_{1.9}PS_{11.8}$ as SSEs in ASSB full cells.[47,56] In addition, such thiostannate based SSEs exhibit broad electrochemical windows, e.g., no redox reactions occur for $Na_{11}Sn_2PS_{12}$ vs. Na^+/Na between 0.3–3.2 V.[47,65] The preparation of such SSEs is mainly performed applying classic high-temperature solid-state methods or sintering processes of appropriate

precursors at high temperatures. The directed removal of crystal water molecules from hydrated solids is an elegant alternative synthetic approach. This was also applied for $Na_3SbS_4{\cdot}9H_2O$ yielding dehydrated Na_3SbS_4[52] with remarkable high ionic conductivity and an excellent electrochemical stability between 0–5.0 V vs. Na^+/Na.[52] However, hydrated thiostannates comprising transition metal complexes or organic cations are often irreversibly destroyed during removal of water molecules, and thus suitable "pure" inorganic crystal water containing compounds have to be identified as possible candidates for Na^+ ion conductors like already demonstrated for the lighter homologue Li. A prominent example is $Na_4SnS_4{\cdot}14H_2O$ which was reported already decades ago. Here, we report on the thermal properties of this compound, the crystal structure of a new metastable polymorph of Na_4SnS_4, the co-decomposition of $Na_4SnS_4{\cdot}14H_2O$ and $Na_3SbS_4{\cdot}9H_2O$, the ionic conduction properties, ^{119}Sn Mössbauer, and ^{23}Na as well as ^{119}Sn magic-angle spinning (MAS) NMR characterization of the materials.

Results and Discussion

The thermal properties of $Na_4SnS_4{\cdot}14H_2O$ (**I**) were investigated using simultaneously thermogravimetry (TG) and differential thermoanalysis (DTA). Upon heating **I** to 300 °C, two steps are observed in the TG curve accompanied by intense and broad endothermic events in the DTA curve (T_p = 66 and 142 °C) (Figure 1a). The mass loss of 42.4 % at 170 °C matches well with that calculated for the removal of all H_2O molecules (42.6 %), which is confirmed by ^{1}H MAS NMR (Figure S1). The X-ray powder diffraction (XRPD) pattern of the product obtained at 300 °C (Figure S2) is dominated by reflections of a new compound with composition Na_4SnS_4 (**II**) with small amounts (≈4 wt %) of literature known Na_4SnS_4 (**III**), which was prepared at elevated temperatures.[8] A second thermal experiment was stopped at 170 °C and the XRPD pattern reveals only reflections of **II** (Figure 1b). A suitable structural model for **II** was refined via Rietveld method (Figure 1c, details in Supporting Information). The preparation of phase-pure **II** is scalable, as confirmed by further syntheses using an inert gas furnace.

We hypothesize that **II** formed by heating of **I** with a rate of 4 K min^{-1} up to 170 °C is kinetically stabilized. Hence, **I** was heated to 300 °C with a lower heating rate of 1 K min^{-1} (Figure 2a) exhibiting significant differences in the TG curve compared to that recorded with 4 K min^{-1}, showing at least three not well resolved reaction steps accompanied by two broad endothermic events in the DTA curve (T_p = 62 and 92 °C). The weight loss (41.4 %) is already finished at

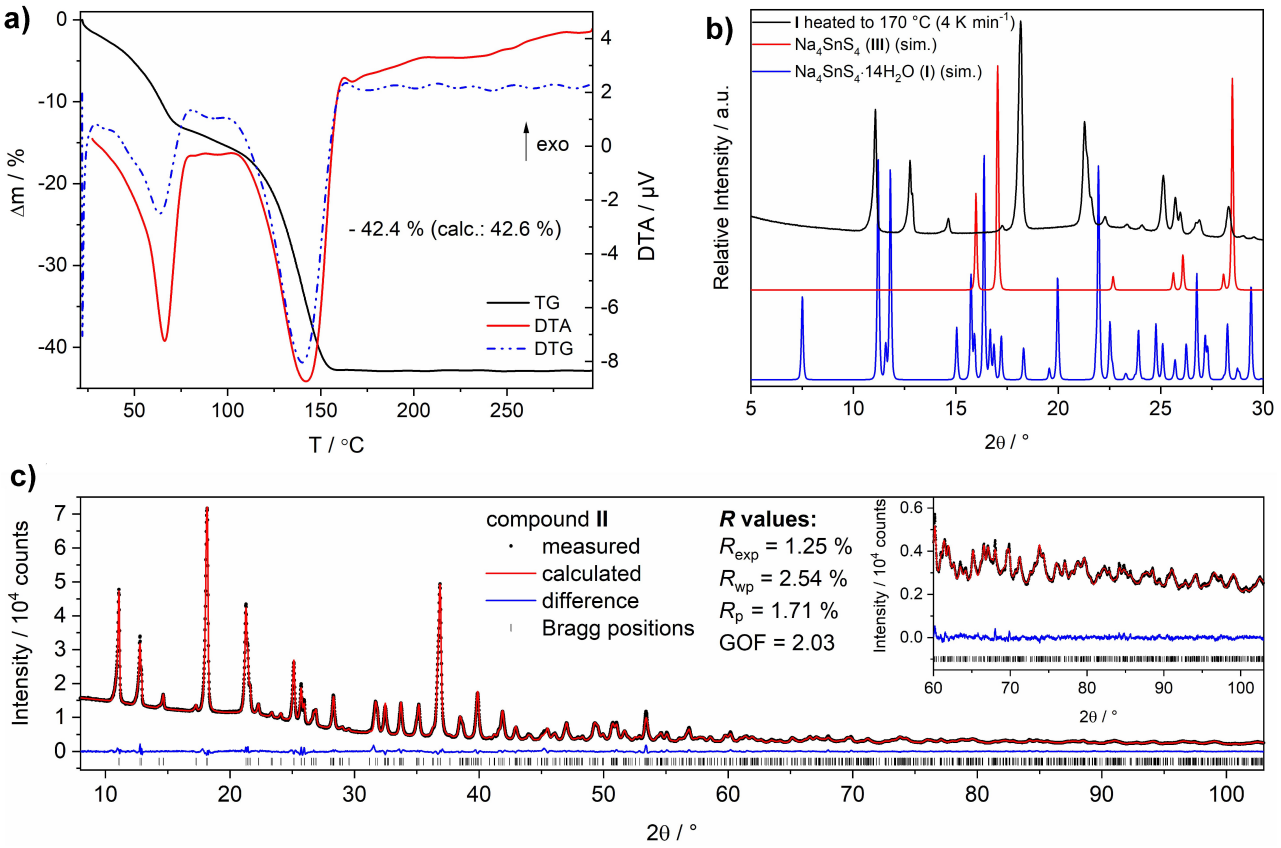

Figure 1. a) TG, DTA and derivative TG (DTG) curves of **I** (heating rate: 4 K min^{-1}, N_2 atmosphere); b) XRPD pattern of a TG product of **I** recovered at 170 °C (4 K min^{-1}) compared to simulated (sim.) patterns of the known Na_4SnS_4 polymorph (**III**) and of **I**; c) final Rietveld plot revealing the new polymorph Na_4SnS_4 (**II**), the inset shows a magnification at high angles.

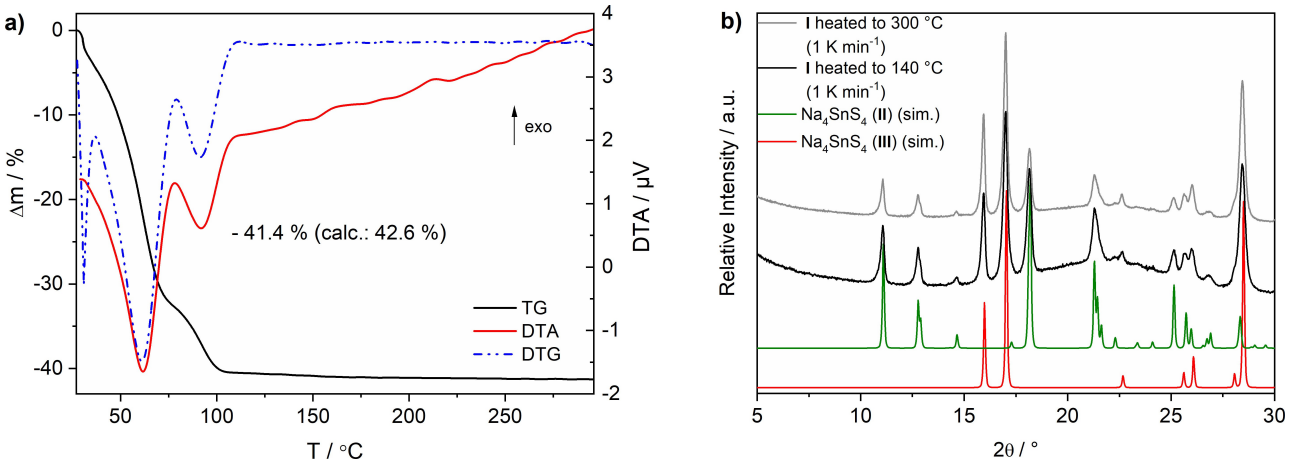

Figure 2. a) TG, DTA and DTG curves of **I** (heating rate: 1 K min^{-1}, N_2 atmosphere); b) XRPD patterns of TG products of **I** recovered at 140 and 300 °C (1 K min^{-1}) compared to simulated (sim.) patterns of the known (**III**) and the new (**II**) polymorph of Na_4SnS_4.

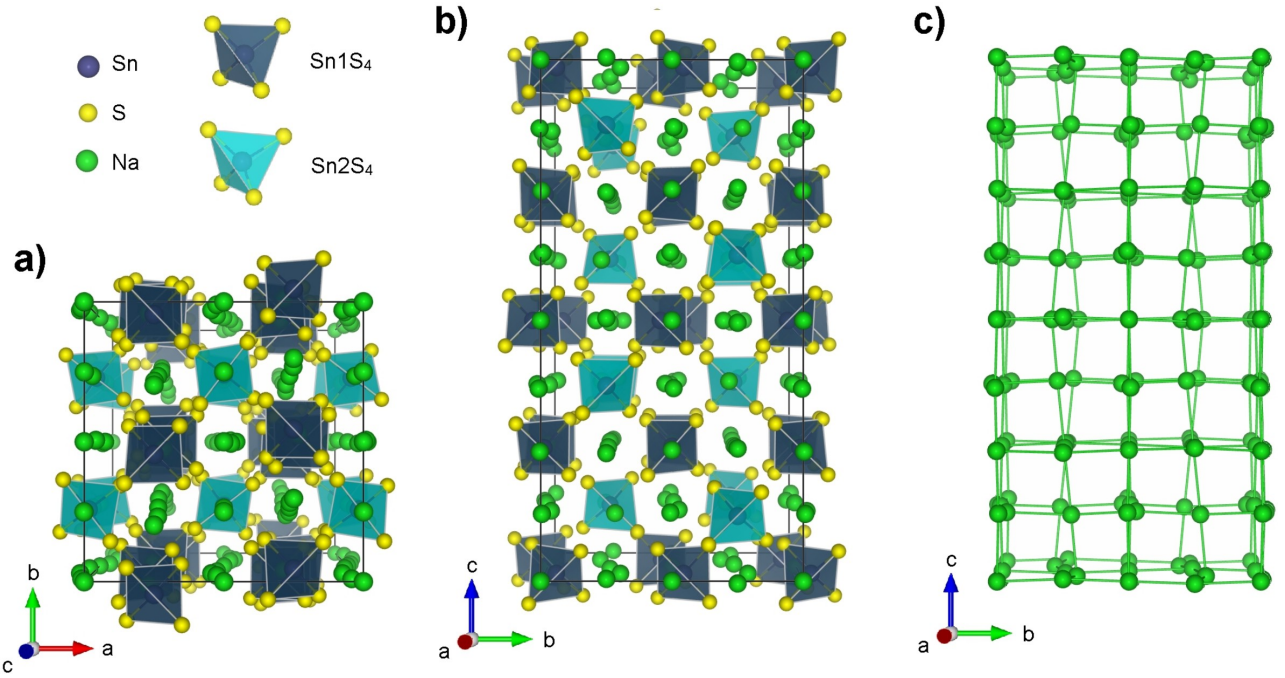

Figure 3. Structure of **II**: Unit cell a) along [001], b) along [100] (note: Na–S bonds are hidden), c) Na···Na contacts < 3.6 Å.

≈105 °C in reasonably good agreement with the emission of all crystal water molecules. A second TG run was performed to 140 °C and independent from the final temperature (140 or 300 °C), the XRPD patterns show reflections of **II** and of **III** (Figure 2b). Quantitative analyses (Figure S3) reveal that the amount of **III** increases during heating from ≈54 wt % at 140 °C to ≈67 wt % at 300 °C, thus the kinetically stabilized polymorph **II** transforms into **III**.

Further TG experiments were performed up to 620 °C and 700 °C (heating rate: 1 K min^{-1}) showing a broad exothermic event at T_p = 563 °C (Figure S4). The XRPD patterns (Figure S5) are now dominated by reflections of **III** (≈95 wt % in TG product recovered at 700 °C, Figure S6). These investigations evidence that **III** is the thermodynamically stable polymorph over the entire temperature range.

The new Na_4SnS_4 polymorph (**II**) crystallizes in the tetragonal space group (SG) $I4_1/acd$ (no. 142) with a = 13.8413(2), c = 27.4232(4) Å, V = 5253.80(12) Å^3 and Z = 24 (Table S1 and S2).[66] The overall structural features are similar to those reported for $Na_{11}Sn_2PS_{12}$,[48–50] and $Na_{11}Sn_2SbS_{12}$.[50,56] The structure of **II** (Figure 3) comprises two unique Sn atoms located on special positions, three crystallographically independent S atoms on general positions, four Na atoms on special positions, and one Na atom on a general position (Table S2). A sixth "interstitial" Na site in loose coordination to eight S atoms ("Na6 void" in Figure S7), which is partially occupied in $Na_{11}Sn_2MS_{12}$ (M =

Sb and P),[47,48,50,67] is not detected for **II**. One has to keep in mind that reliable information about low-level occupation of light elements can hardly be extracted from in-house XRPD data. Both Sn^{4+} cations are tetrahedrally coordinated by S^{2-} anions and **II** can be described as $Na_{12}[SnS_4]_2\{SnS_4\}$ with Sn1 located in $[SnS_4]$ (Table S6, dark blue in Figure 3) and Sn2 in $\{SnS_4\}$ (light blue in Figure 3), respectively. According to literature, P and Sb are located on a special position in $Na_{11}Sn_2PS_{12}$ and $Na_{11}Sn_2SbS_{12}$ and substitution of Sn^{4+} by $>1/3$ P^{5+} or Sb^{5+} leads to formation of additional phases (e.g. Na_3PS_4 or Na_3SbS_4)[48–50,56] or results in another crystal structure (e.g. $Na_{10}SnP_2S_{12}$).[68] Using a general notation $Na_{12-3y-3x}[SnS_4]_2\{Sn_{1-3y-3x}P_{3y}Sb_{3x}S_4\}$, corresponding to the formula $Na_{4-y-x}Sn_{1-y-x}P_ySb_xS_4$, **II** can be described as the new pure thiostannate ($x=0$, $y=0$) of this structural family.

Na–S distances are observed at 2.7–3.3 Å (Table S6) and a distance gap occurs between 3.3 and 3.7 Å (Figure S10) for **II**, indicating that ionic bonding interactions are present <3.3 Å and very weak interactions in an enlarged environment. Taking the sum of ionic radii as a limit for ionic bonds, the Na^+ cations are in three different coordination environments (Table S6): Na1 is in a distorted trigonal-bipyramidal S^{2-} coordination (Na–S between 2.849–3.189 Å), and a sixth S^{2-} anion is located at Na1···S1: 3.810 Å. Na2 is tetrahedrally surrounded by S^{2-} (Na–S: 2.793–2.924 Å) with additional weak interactions to two S^{2-} (Na2···S2: 3.696 Å). Na3, Na4, and Na5 are in a highly distorted octahedral geometry of S^{2-} (Na–S: 2.719–3.270 Å). Considering also weak interactions <4 Å, all Na^+ cations are located in highly distorted NaS_6 octahedra. Noticeably, the longest Na···S distance in these NaS_6 polyhedra is distinctly larger for **II** (Na1–S1: 3.810 Å), than those reported for $Na_{11}Sn_2MS_{12}$ (M = Sb and P, Na···S ≤ 3.572 Å and ≤ 3.361 Å, respectively).[50]

A three-dimensional network is generated by edge- and corner-sharing of NaS_x polyhedra, and a detailed description of interconnections is given in the Supporting Information (see Figure S7). This network exhibits nearly linear and zig-zag Na^+ cation chains along the *c*-axis and in the *ab*-plane (Figure 3a and b) with interatomic Na···Na distances of 3.297–3.593 Å (Figure 3c, Table S6). Each Na^+ is in almost square planar environment of four Na^+, leading to a distorted NbO-topology substructure prominent for, e.g., $Na_{11}Sn_2PS_{12}$.[48,67]

The literature known Na_4SnS_4 polymorph (**III**) crystallizes in the tetragonal SG $P\bar{4}2_1c$ (no. 114) with $a=7.84679(3)$ and $c=6.95798(4)$ Å, $V=428.42(1)$ Å^3 and $Z=2$ (Tables S1, S5), close to values already reported.[8,69] In this structure (Figure 4, $2\times2\times4$ unit cells for comparability with **II**) all Sn^{4+} cations are located on one special position and are tetrahedrally coordinated by S^{2-} (Sn–S: 2.380 Å). The Na^+ cations are located on one general position and are surrounded by five S^{2-} (Na–S: 2.809–3.113 Å, Table S7). These NaS_5 units are linked by sharing common edges and joined to the SnS_4 tetrahedra by edge-sharing. In contrast to **II**, several Na^+ cations are located in the voids between SnS_4 units. The Na···Na contacts in **III** (Figure 4c) are similar in the *ab*-plane (3.425–3.534 Å) to those in **II** (3.463–3.525 Å), but significantly longer along the *c*-axis (dotted lines in Figure 4c) (**III**: 3.669 Å vs. **II**: 3.293 and 3.595 Å, see Figure S11).

Applying the same fast and moderate temperature approach as for **II** ($x=0$), samples containing Sb (**IIa**, $x=0.01$, **IIb** $x=0.10$) were prepared by co-decomposition of stoichiometric amounts of $Na_4SnS_4{\cdot}14\,H_2O$ and

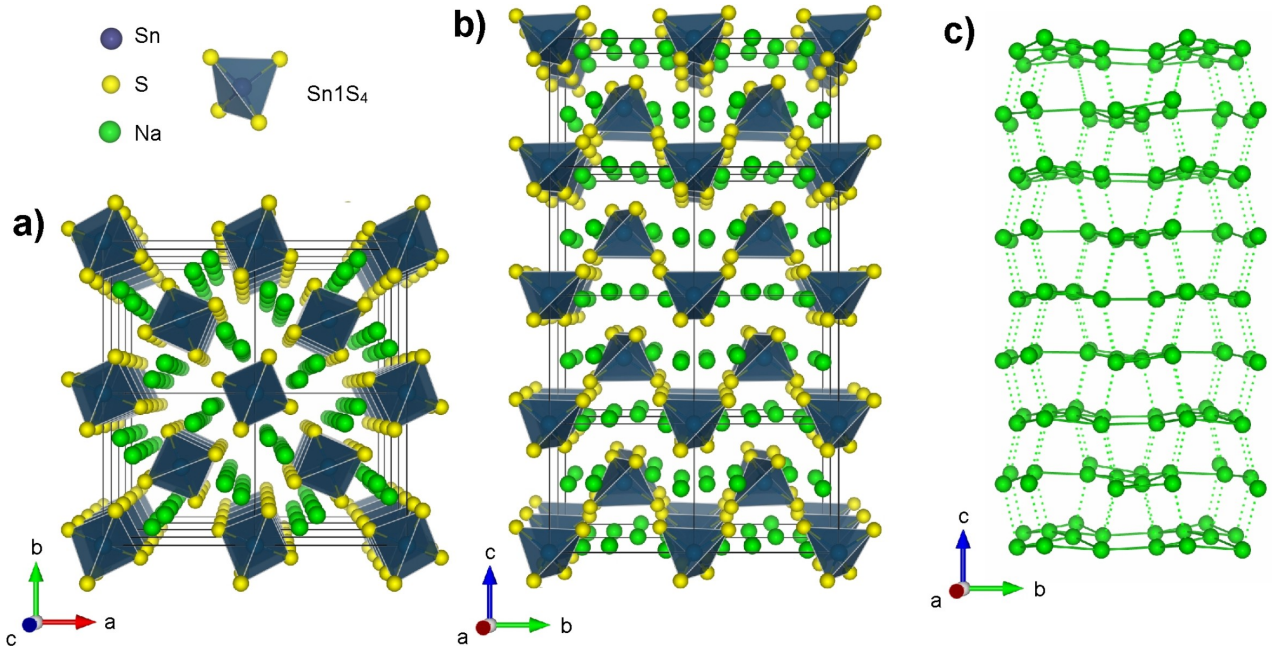

Figure 4. Structure of **III**: $2\times2\times4$ unit cells a) along [001], b) along [100] (note: Na–S bonds are hidden), c) Na···Na connections (dotted lines represent connections >3.6 Å).

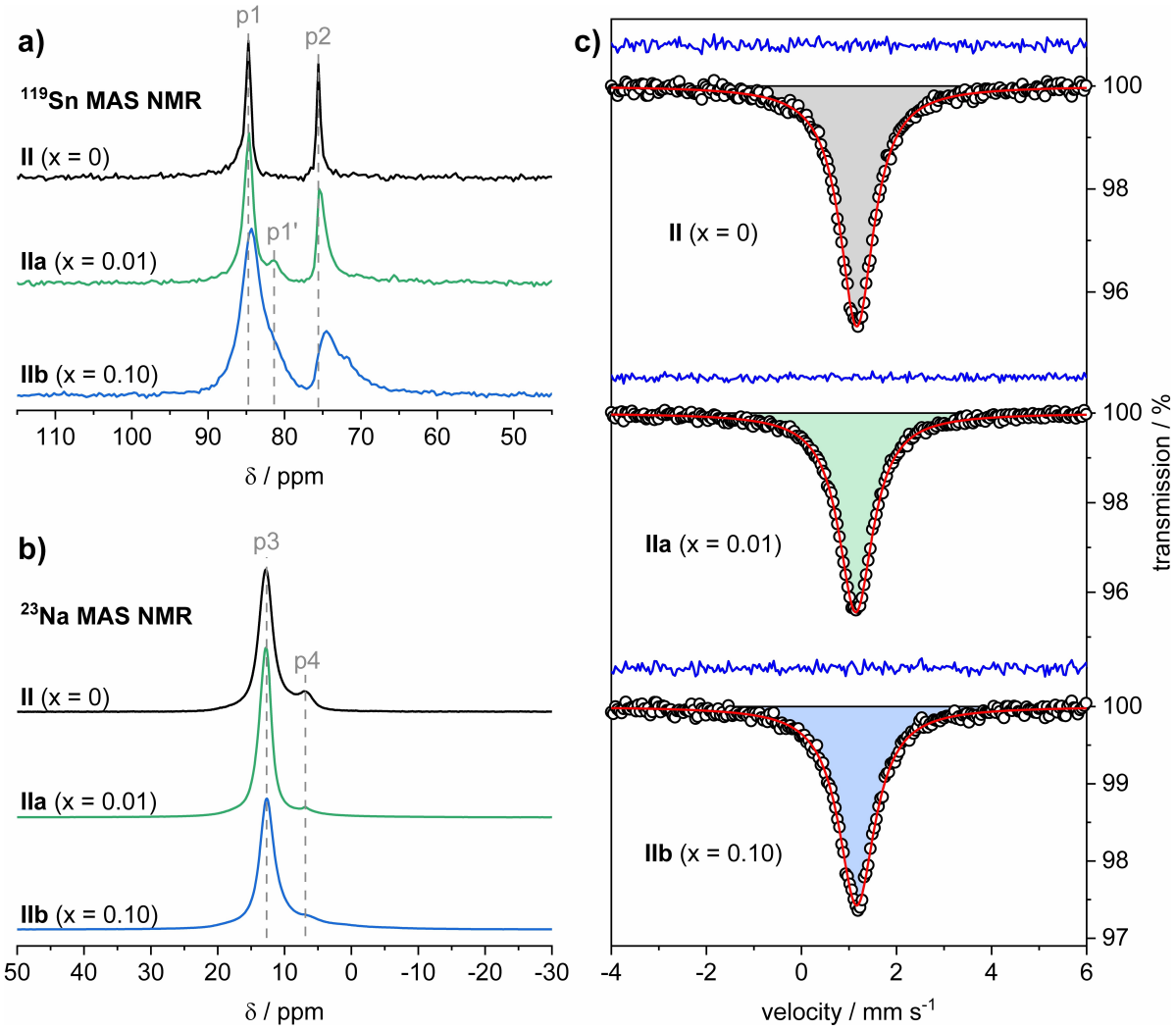

Figure 5. a) ^{119}Sn MAS NMR, b) ^{23}Na MAS NMR, and c) ^{119}Sn Mössbauer spectra for **II**, **IIa**, and **IIb** ($Na_{4-x}Sn_{1-x}Sb_xS_4$, $x = 0$, 0.01, 0.10).

$Na_3SbS_4 \cdot 9H_2O$ at 170 °C (details in Supporting Information) to obtain $Na_{4-x}Sn_{1-x}Sb_xS_4$ with low Sb contents.

Rietveld refinements (Figure S8) reveal that this easy, scalable, and cost-effective synthetic approach yields phase-pure products **IIa** and **IIb** crystallizing isostructurally to **II** in $I4_1/acd$ with lattice parameters $a = 13.8399(3)$ and 13.8284 (3) Å, $c = 27.4273(8)$ and 27.4679(8) Å, $V = 5253.51(22)$ and 5252.55(24) Å^3, respectively (Tables S1, S3 and S4),[66] in good agreement with values reported for, e.g., $Na_{3.95}Sn_{0.95}Sb_{0.05}S_4$ ($a = 13.8362$ Å, $c = 27.4499$ Å, $V = 5255$ Å^3).[56] The lattice parameters for **IIa** are between those for **II** and **IIb** (Figure S9), evidencing that even the substitution of only $x = 0.01$ was successful. Some structural features should be discussed for this solid solution with increasing Sb content: i) expansion of the unit cell along the *c*-axis and contraction in the *ab*-plane (Figure S9); ii) a narrower gap between near and far Na–S distances assuming highly distorted NaS_6 octahedra with the longest distance in all NaS_6 polyhedra to be 3.810, 3.754, and 3.666 Å for $x = 0$, 0.01, and 0.10 (Figure S10 and Table S6); iii) a more uniform distribution of distances along the *c*-axis in the NbO-like Na^+ cation sublattice (longest-shortest Na···Na separation: 0.30, 0.23, and only 0.04 Å for $x = 0$, 0.01, and 0.10, Figure S11, Table S6); iv) only small changes (< 0.03 Å) of Na···Na separations in the *ab*-plane (Figure S11, Table S6).

The local environments of Sn^{4+} and Na^+ cations in **II**, **IIa**, and **IIb** were further investigated by solid-state ^{119}Sn and ^{23}Na MAS NMR (Figure 5a and b, also Figure S12) and ^{119}Sn Mössbauer spectroscopy (Figure 5c). Parameters derived from these experiments are given in Table 1. The ^{119}Sn MAS

Table 1: Results of ^{119}Sn and ^{23}Na MAS NMR and ^{119}Sn Mössbauer spectroscopy for **II**, **IIa**, and **IIb** ($Na_{4-x}Sn_{1-x}Sb_xS_4$, $x = 0$, 0.01, 0.10): chemical shift δ, isomer shift IS, and line width Γ.

	^{119}Sn MAS NMR δ [ppm]			^{23}Na MAS NMR δ [ppm]		^{119}Sn Mössbauer IS [mm s^{-1}]	Γ [mm s^{-1}]
peaks	p1	p1′	p2	p3	p4		
II	84.7(1)	–	75.6(1)	12.8(1)	6.9(1)	1.17(1)	0.87(1)
IIa	84.6(1)	81.4(1)	75.5(1)	12.8(1)	6.9(1)	1.14(1)	0.88(1)
IIb	84.3(1)	81 to 83	74.5(1)	12.7(1)	≈6.9	1.16(1)	0.93(1)

NMR spectrum (Figure 5a) for **II** exhibits two peaks at 84.7(1) (p1) and 75.6(1) ppm (p2) with an intensity ratio of A_{p1}:$A_{p2} \approx 2:1$. Hence, p1 is assigned to Sn^{4+} cations on the crystallographic Sn1 site and p2 to those located on the Sn2 site. The chemical shifts are comparable to values reported for SnS_4 tetrahedra in the solid polymorph **III**[70] and for $[SnS_4]^{4-}$ units in the liquid-state.[71,72] With increasing Sb content (**IIa** and **IIb**), a shift of p1 and p2 to lower values, broader signals, and a higher degree of peak asymmetry is observed. Additionally, a third peak (p1′) close to p1 appears. These observations point towards an increased shielding around Sn^{4+} cations and local distortion of the polyhedra caused by Sb^{5+} cations in the nearby environment. An intensity ratio of $A_{p1+p1'}$: $A_{p2} \approx 2:1$ is determined for all samples, leading to the conclusion, that p1′ represents Sn^{4+} cations on the Sn1 site which are in close proximity to Sb^{5+} cations, thus being in a different local environment than Sn^{4+} cations close to other Sn^{4+} cations only. In all ^{23}Na MAS NMR spectra (Figure 5b), two peaks at ≈12.8 (p3) and ≈6.9 ppm (p4) are detected. No ^{23}Na MAS NMR data is reported for $Na_{11}Sn_2SbS_{12}$, but a single and sharp ^{23}Na MAS NMR signal is observed for $Na_{11}Sn_2PS_{12}$[48] and $Na_{11.1}Sn_{2.1}P_{0.9}Se_{12}$,[43] despite six crystallographically distinct Na sites, resulting from fast ionic motion in the NMR time frame. We assume a comparable situation for $Na_{4-x}Sn_{1-x}Sb_xS_4$. A distinctly lower peak intensity of p4 in **IIa** and **IIb** compared to **II** is a good hint that more Na^+ cations participate in the ion motion if Sn^{4+} is substituted by Sb^{5+}.

All ^{119}Sn Mössbauer spectra (Figure 5c) can be well fitted with a singlet with isomer shifts in the range 1.15(1) mm s^{-1} and a full width at half maximum of about 0.9 mm s^{-1}. Similar values have been reported for **III**[6] and $Li_{10}SnP_2S_{12}$.[73] This peak is thus assigned to Sn^{4+} cations in the tetrahedral S^{2-} environments. The different Sn environments in the crystal structure are too similar to be discriminated by Mössbauer spectroscopy. Nonetheless, the spectra show a broadening of the line for the sample with the highest Sb content (**IIb**) indicating a local structural distortion in good agreement with the ^{119}Sn MAS NMR results.

The structural features observed for **II**, **IIa**, and **IIb** promise a potential application as SSEs in ASSBs. Hence, the Na^+ cation conductivities were determined by electrochemical impedance spectroscopy (EIS) between −10 to +70 °C. Representative results are shown in Figure 6. In the Nyquist plots recorded at 0 °C (Figure 6a) for **II**, **IIa**, and **IIb**, single depressed semicircles and sloping lines at small frequencies are observed. The deconvolution of contributions from bulk and grain boundaries is not possible and all AC impedance spectra were fitted with an equivalent circuit as shown in Figure 6b (details in Supporting Information). The Na^+ cation conductivities σ and capacitances C at different temperatures are shown in Table 2. Values for C correspond to averaged bulk and grain boundary transport behavior if compared to empirical characteristics reported in ref. [74] ($C_{bulk} \approx 0.001$ nF, $C_{grain\ boundary} \approx 4$ nF). The EIS experiments demonstrate good (**II**) to superior (**IIb**) Na^+ cation motion in the whole temperature regime with σ covering several orders of magnitude. The substitution of Sn^{4+} by Sb^{5+} has a highly beneficial impact on the Na^+ cation motion and σ of **II** is already enhanced by one order of magnitude for $x = 0.01$ (e.g. $\sigma(\mathbf{II})_{30°C} = 3.0$ μS cm^{-1}, $\sigma(\mathbf{IIa})_{30°C} = 26$ μS cm^{-1}) despite it is isostructural. For $x = 0.10$, σ is >40 times larger than for **II** ($\sigma(\mathbf{IIb})_{30°C} = 0.1$ mS cm^{-1}) enabling superionic conduction properties comparable to findings for high-temperature products of $Na_{4-x}Sn_{1-x}Sb_xS_4$ (e.g. $\sigma_{30°C} \approx 0.1$ mS cm^{-1} for $Na_{3.95}Sn_{0.95}Sb_{0.05}S_4$).[56] In contrast, the AC resistance for **III** is too high for a reasonable determination of σ at $T < 25$ °C. Even at $T \geq 25$ °C, only approximate values for σ can be calculated (inset in Figure 6b), similar to those reported for **III**.[69] σ is at least two orders of magnitude lower in **III** ($\sigma(\mathbf{III})_{30°C} \approx 0.02$ μS cm^{-1}) compared to **II**.

Table 2: Ionic conductivities σ and capacitances C at various temperatures for **II**, **IIa**, **IIb** ($Na_{4-x}Sn_{1-x}Sb_xS_4$, $x = 0$, 0.01, 0.10), and **III** (Na_4SnS_4).

T [°C]	σ [μS cm^{-1}]				C [nF]			
	II	**IIa**	**IIb**	**III**[a]	**II**	**IIa**[b]	**IIb**[b]	**III**[a]
70	24.4(6)	124(19)	626(14)	0.25(3)	0.05(1)	–	–	0.06(1)
60	15.4(2)	90.7(77)	443(3)	0.15(2)	0.05(1)	–	–	0.06(1)
50	9.33(4)	62.1(30)	297(2)	0.08(1)	0.06(1)	–	–	0.06(1)
40	5.45(3)	40.8(14)	196(5)	0.04(1)	0.06(1)	–	–	0.06(1)
30	3.02(3)	25.5(6)	123(3)	0.02(1)	0.06(1)	0.08(1)	–	0.06(1)
25	2.21(3)	19.9(4)	95.3(11)	0.01(1)	0.06(1)	0.08(1)	–	0.07(1)
20	1.60(3)	15.3(2)	73.6(6)	–	0.07(1)	0.08(1)	0.14(1)	–
10	0.79(2)	8.76(1)	42.1(2)	–	0.07(1)	0.09(1)	0.14(2)	–
0	0.37(1)	4.72(1)	23.2(1)	–	0.07(1)	0.09(1)	0.16(1)	–
−10	0.17(1)	2.37(1)	12.1(2)	–	0.07(1)	0.10(1)	0.19(1)	–

[a] EIS spectra <25 °C are too noisy for reliable calculations. [b] C(**IIa**) and C(**IIb**) cannot be extracted at ≥40 and ≥25 °C, respectively (indistinct semicircles).

The temperature-dependent σ follow the Arrhenius law for all samples (Figure 6c). The activation energy E_a is 0.65 eV for **III** comparable to literature data (0.58 eV)[69] and larger than for **II** (0.51 eV). Substitution of Sn^{4+} by Sb^{5+} reduces E_a to 0.41 eV for **IIa** and **IIb** close to data reported for superionic conductors, e.g., $Na_{11}Sn_2PS_{12}$ (0.39 eV,[48] 0.25 eV[49]), $Na_{10}SnP_2S_{12}$ (0.36 eV[68]), $Na_{11}Sn_2SbS_{12}$ (0.34 eV[50]), Na_3PS_4 (0.38 eV, 0.35 eV),[45] and Na_3SbS_4 (0.25 eV,[51] 0.22 eV[52]).

The results from EIS highlight the pronounced impact of structural differences, in particular the different three-dimensional Na^+ cation topology on the ion motion properties comparing **II** and **III**. Moreover, the significantly enhanced Na^+ cation mobility with increasing Sb content in $Na_{4-x}Sn_{1-x}Sb_xS_4$ needs to be discussed. One reason is certainly the lower total Na occupation inevitably coming along with the substitution, hence statistically more vacant sites are present for Na^+ ion hopping. Another reason is the more regular distribution of Na···Na connections with increasing Sb content (Figure S11), being beneficial for the ionic conduction along the *c*-axis. One bottleneck debated for the ionic conduction in $Na_{4-y-x}Sn_{1-y-x}P_ySb_xS_4$ is the Na^+ cation hopping through a Na6 void (see Figure S7) limited by the shortest S···S distances between shared faces of $Na6S_8$

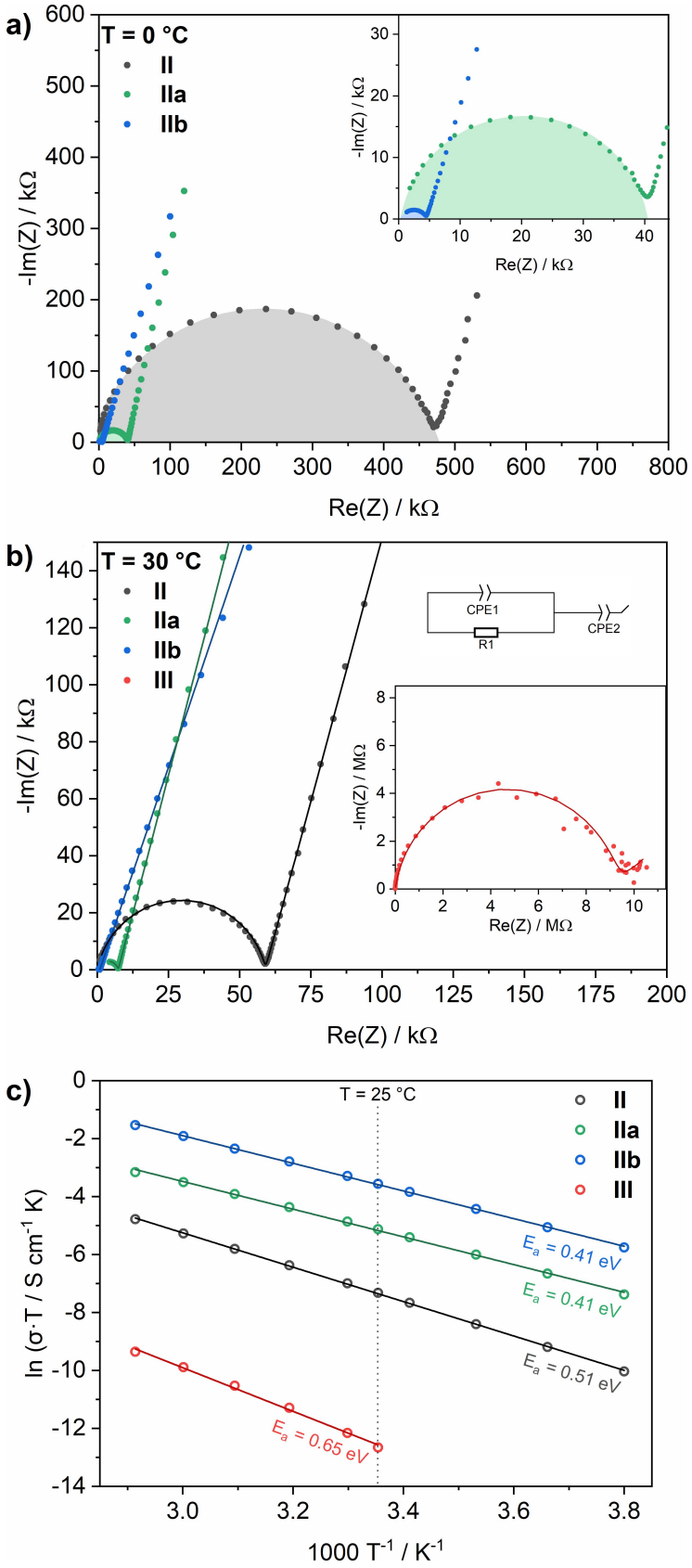

Figure 6. Nyquist plots recorded at a) 0 °C and b) 30 °C; c) Arrhenius plots for **II**, **IIa**, **IIb** ($Na_{4-x}Sn_{1-x}Sb_xS_4$, $x = 0$, 0.01, 0.10), and **III** (Na_4SnS_4). An equivalent circuit for these AC impedance spectra is shown in (b).

and $Na1S_6$ or $Na2S_6$ (Figure S13).[50] The S···S barrier for the Na1→Na6→Na1 pathway is almost the same (±0.01 Å) and increases only slightly (+0.06 Å) for the Na2→Na6→Na2 pathway if Sn^{4+} is replaced by Sb^{5+} (Table S8). These small changes in contradiction to the tremendously different ionic conductivity in this series confirm the previous observations that these pathways are less important for the ionic conduction in this structural family.[50]

Additionally, the paddle-wheel mechanism is long-debated for superionic conductors, e.g., explaining an enhanced Na^+ cation conduction property for $Na_{11}Sn_2PS_{12}$ vs. $Na_{11}Sn_2SbS_{12}$ by less hindered PS_4 rotational dynamics compared to those of SbS_4 units.[75] The results of NMR and Mössbauer experiments indicate larger SnS_4 distortions and improved Na^+ cation mobility with increasing Sb content, in agreement with the EIS results. However, calculations and modeling are now necessary to understand the SnS_4 dynamics, its relation to SbS_4 incorporation and Na^+ mobility.

To this end, we performed quantum calculations to elucidate the role of $[SnS_4]^{4-}$ and $[SbS_4]^{3-}$ tetrahedrons for coordinating interstitial Na^+ ions. As a proxy model featuring Na^+ coordination by the edges of two MS_4 motifs, we characterized Na^+ ion incorporation between two charge neutral $Na_4[SnS_4]$ species. This was compared to Na^+ incorporation between adjacent $Na_4[SnS_4]$ and $Na_3[SbS_4]$ tetrahedrons. Strikingly, we find latter scenario (i.e. the $[Na_4[SnS_4]$-Na-$[SbS_4]Na_3]^+$ hetero-pair) to be preferred by 0.3 eV, hence suggesting significant lowering of the interstitial formation energy. This may be rationalized by the larger formal charge of the Sb^{5+} species that gives rise to the more compact SbS_4 tetrahedron as compared to SnS_4—with the Sb–S and Sn–S distances being 2.53 and 2.44 Å, respectively (see Supporting Information for details of the quantum calculations). Thus, SbS_4 incorporation in $Na_{4-x}Sn_{1-x}Sb_xS_4$ offers additional space to the neighboring SnS_4 tetrahedrons—which is suggested to not only facilitate rotation in support of Na^+ hopping, but also helps Frenkel defect formation (producing Na vacancies as the suggested mobile species).

Conclusion

Here we demonstrated that the new, kinetically stabilized Na_4SnS_4 polymorph is obtained via directed removal of crystal water from $Na_4SnS_4{\cdot}14H_2O$ at 170 °C. This process at relatively moderate temperature is very easy, cost-effective, and scalable, and also provides an economic preparation method for the solid solution $Na_{4-x}Sn_{1-x}Sb_xS_4$ by co-decomposition with $Na_3SbS_4{\cdot}9H_2O$. In contrast to recent claims in literature, we here report that this solid solution exhibits no lower Sb limit using the presented syntheses, but slow heating to higher temperatures inevitable causes structural transformation of the new Na_4SnS_4 polymorph into the known, thermodynamically stabilized form. These findings enabled a systematic study at the lower Sb substitution boundary for the first time. Combined XRPD, ^{23}Na and ^{119}Sn NMR, ^{119}Sn Mössbauer, and EIS experiments shed light on the local and crystallographic structure for $x=0$, 0.01, and 0.10 and their relation to the Na^+ cation mobility. Compared to the known Na_4SnS_4 polymorph, the room temperature Na^+ conductivity of the new form is considerably improved by two orders of magnitude to $\sigma_{25°C}=2\times10^{-3}$ mS cm^{-1}. Incorporation of minor Sb^{5+} amounts ($x=0.01$) in the new polymorph already enhances the Na^+ conductivity significantly and further substitution to $x=0.10$ enables room temperature superionic conduction properties ($\sigma_{25°C}=0.1$ mS cm^{-1}, $E_a=0.41$ eV). The synthetic approach presented here opens new avenues to syntheses of SSE by thermal co-decomposition using other precursor mixtures to access compounds of this thiostannate family with methodical low-level cation and anion doping, e.g., by incorporation of P^{5+}, Sb^{5+}, Cl^-, and Br^- in Na_4SnS_4,[76] which was difficult until now because of the temperature-dependent polymorphism.

Acknowledgements

Financial support by the State of Schleswig-Holstein is gratefully acknowledged. We thank Aleksej Jochim, Carsten Wellm, and Inke Jess for TG measurements. We gratefully thank Lina Liers for attempting additional electrochemical experiments. Open Access funding enabled and organized by Projekt DEAL.

Conflict of Interest

The authors declare no conflict of interest.

Data Availability Statement

The data that support the findings of this study are available from the corresponding author upon reasonable request.

Keywords: Mössbauer Spectroscopy · Na^+ Ionic Conductivity · NMR Spectroscopy · Thermal Co-Decomposition · X-Ray Diffraction

[1] W. Schiwy, S. Pohl, B. Krebs, *Z. Anorg. Allg. Chem.* **1973**, *402*, 77–86.
[2] B. Krebs, S. Pohl, W. Schiwy, *Z. Anorg. Allg. Chem.* **1972**, *393*, 241–252.
[3] J. H. Liao, C. Varotsis, M. G. Kanatzidis, *Inorg. Chem.* **1993**, *32*, 2453–2462.
[4] B. Krebs, W. Schiwy, *Z. Anorg. Allg. Chem.* **1973**, *398*, 63–71.
[5] W. S. Sheldrick, B. Schaaf, *Z. Anorg. Allg. Chem.* **1994**, *620*, 1041–1045.
[6] R. Greatrex, N. N. Greenwood, M. Ribes, *J. Chem. Soc. Dalton Trans.* **1976**, 500–504.
[7] Y. Ko, C. L. Cahill, J. B. Parise, *J. Chem. Soc. Chem. Commun.* **1994**, 69–70.
[8] J.-C. Jumas, E. Philippot, F. Vermot-Gaud-Daniel, M. Ribes, M. Maurin, *J. Solid State Chem.* **1975**, *14*, 319–327.

[9] B. Seidlhofer, N. Pienack, W. Bensch, *Z. Naturforsch. B* **2010**, *65*, 937–975.
[10] M. Behrens, M.-E. Ordolff, C. Näther, W. Bensch, K.-D. Becker, C. Guillot-Deudon, A. Lafond, J. A. Cody, *Inorg. Chem.* **2010**, *49*, 8305–8309.
[11] Z. Hassanzadeh Fard, C. Müller, T. Harmening, R. Pöttgen, S. Dehnen, *Angew. Chem. Int. Ed.* **2009**, *48*, 4441–4444; *Angew. Chem.* **2009**, *121*, 4507–4511.
[12] H. P. Nayek, W. Massa, S. Dehnen, *Inorg. Chem.* **2008**, *47*, 9146–9148.
[13] G. A. Marking, M. Evain, V. Petricek, M. G. Kanatzidis, *J. Solid State Chem.* **1998**, *141*, 17–28.
[14] M. Suseela Devi, K. Vidyasagar, *J. Chem. Soc. Dalton Trans.* **2002**, 2092–2096.
[15] C. L. Teske, *Z. Anorg. Allg. Chem.* **1978**, *445*, 193–201.
[16] C. L. Teske, H. Terraschke, S. Mangelsen, W. Bensch, *Z. Anorg. Allg. Chem.* **2020**, *646*, 1716–1721.
[17] C. L. Teske, *Z. Anorg. Allg. Chem.* **1980**, *460*, 163–168.
[18] A. Kumari, K. Vidyasagar, *J. Solid State Chem.* **2007**, *180*, 2013–2019.
[19] R.-H. Duan, P.-F. Liu, H. Lin, S.-X. Huangfu, L.-M. Wu, *Dalton Trans.* **2017**, *46*, 14771–14778.
[20] N. Pienack, W. Bensch, *Z. Anorg. Allg. Chem.* **2006**, *632*, 1733–1736.
[21] N. Pienack, K. Möller, C. Näther, W. Bensch, *Solid State Sci.* **2007**, *9*, 1110–1114.
[22] N. Pienack, C. Näther, W. Bensch, *Solid State Sci.* **2007**, *9*, 100–107.
[23] B. Zhang, M.-L. Feng, J. Li, Q.-Q. Hu, X.-H. Qi, X.-Y. Huang, *Cryst. Growth Des.* **2017**, *17*, 1235–1244.
[24] N. Pienack, A. Puls, C. Näther, W. Bensch, *Inorg. Chem.* **2008**, *47*, 9606–9611.
[25] N. Pienack, C. Näther, W. Bensch, *Z. Naturforsch. B* **2008**, *63*, 1243–1251.
[26] X.-H. Qi, K.-Z. Du, M.-L. Feng, J.-R. Li, C.-F. Du, B. Zhang, X.-Y. Huang, *J. Mater. Chem. A* **2015**, *3*, 5665–5673.
[27] D.-X. Jia, J. Dai, Q.-Y. Zhu, Y. Zhang, X.-M. Gu, *Polyhedron* **2004**, *23*, 937–942.
[28] Q. Zhao, D. Jia, Y. Zhang, L. Song, J. Dai, *Inorg. Chim. Acta* **2007**, *360*, 1895–1901.
[29] D.-X. Jia, A.-M. Zhu, J. Deng, Y. Z. Suzhou, *Z. Anorg. Allg. Chem.* **2007**, *633*, 1246–1250.
[30] J. Han, Y. Liu, J. Lu, C. Tang, F. Wang, Y. Shen, Y. Zhang, D. Jia, *Inorg. Chem. Commun.* **2015**, *57*, 18–21.
[31] M. S. Hvid, P. Lamagni, N. Lock, *Sci. Rep.* **2017**, *7*, 45822.
[32] M.-L. Feng, D. Sarma, X.-H. Qi, K.-Z. Du, X.-Y. Huang, M. G. Kanatzidis, *J. Am. Chem. Soc.* **2016**, *138*, 12578–12585.
[33] W.-A. Li, J.-R. Li, B. Zhang, H.-Y. Sun, J.-C. Jin, X.-Y. Huang, M.-L. Feng, *ACS Appl. Mater. Interfaces* **2021**, *13*, 10191–10201.
[34] M. S. Hvid, H. S. Jeppesen, M. Miola, P. Lamagni, R. Su, K. M. Ø. Jensen, N. Lock, *IUCrJ* **2019**, *6*, 804–814.
[35] M. Ø. Filsø, I. Chaaban, A. Al Shehabi, J. Skibsted, N. Lock, *Acta Crystallogr. Sect. B* **2017**, *73*, 931–940.
[36] J. Hilbert, C. Näther, W. Bensch, *Z. Anorg. Allg. Chem.* **2017**, *643*, 1861–1866.
[37] J. Hilbert, C. Näther, W. Bensch, *Cryst. Growth Des.* **2017**, *17*, 4766–4775.
[38] A. Benkada, C. Näther, W. Bensch, *Z. Anorg. Allg. Chem.* **2020**, *646*, 1352–1358.
[39] J. Li, B. Marler, H. Kessler, M. Soulard, S. Kallus, *Inorg. Chem.* **1997**, *36*, 4697–4701.
[40] P. Nørby, E. Eikeland, J. Overgaard, S. Johnsen, B. B. Iversen, *CrystEngComm* **2015**, *17*, 2413–2420.
[41] A. Benkada, H. Reinsch, W. Bensch, *Eur. J. Inorg. Chem.* **2019**, 4427–4432.
[42] R. Schlem, P. Till, M. Weiss, T. Krauskopf, S. P. Culver, W. G. Zeier, *Chem. Eur. J.* **2019**, *25*, 4143–4148.
[43] M. Duchardt, S. Neuberger, U. Ruschewitz, T. Krauskopf, W. G. Zeier, J. Schmedt auf der Günne, S. Adams, B. Roling, S. Dehnen, *Chem. Mater.* **2018**, *30*, 4134–4139.
[44] H. Dai, W. Xu, Z. Hu, Y. Chen, X. Wei, B. Yang, Z. Chen, J. Gu, D. Yang, F. Xie, W. Zhang, R. Guo, G. Zhang, W. Wei, *Front. Energy Res.* **2020**, *8*, 97.
[45] T. Krauskopf, S. P. Culver, W. G. Zeier, *Inorg. Chem.* **2018**, *57*, 4739–4744.
[46] A. Hayashi, K. Noi, N. Tanibata, M. Nagao, M. Tatsumisago, *J. Power Sources* **2014**, *258*, 420–423.
[47] Z. Yu, S.-L. Shang, Y. Gao, D. Wang, X. Li, Z.-K. Liu, D. Wang, *Nano Energy* **2018**, *47*, 325–330.
[48] M. Duchardt, U. Ruschewitz, S. Adams, S. Dehnen, B. Roling, *Angew. Chem. Int. Ed.* **2018**, *57*, 1351–1355; *Angew. Chem.* **2018**, *130*, 1365–1369.
[49] Z. Zhang, E. Ramos, F. Lalère, A. Assoud, K. Kaup, P. Hartman, L. F. Nazar, *Energy Environ. Sci.* **2018**, *11*, 87–93.
[50] E. P. Ramos, Z. Zhang, A. Assoud, K. Kaup, F. Lalère, L. F. Nazar, *Chem. Mater.* **2018**, *30*, 7413–7417.
[51] L. Zhang, D. Zhang, K. Yang, X. Yan, L. Wang, J. Mi, B. Xu, Y. Li, *Adv. Sci.* **2016**, *3*, 1600089.
[52] H. Wang, Y. Chen, Z. D. Hood, G. Sahu, A. S. Pandian, J. K. Keum, K. An, C. Liang, *Angew. Chem. Int. Ed.* **2016**, *55*, 8551–8555; *Angew. Chem.* **2016**, *128*, 8693–8697.
[53] A. Banerjee, K. H. Park, J. W. Heo, Y. J. Nam, C. K. Moon, S. M. Oh, S.-T. Hong, Y. S. Jung, *Angew. Chem. Int. Ed.* **2016**, *55*, 9634–9638; *Angew. Chem.* **2016**, *128*, 9786–9790.
[54] H. Gamo, N. H. H. Phuc, R. Matsuda, H. Muto, A. Matsuda, *Mater. Today* **2019**, *13*, 45–49.
[55] A. Hayashi, N. Masuzawa, S. Yubuchi, F. Tsuji, C. Hotehama, A. Sakuda, M. Tatsumisago, *Nat. Commun.* **2019**, *10*, 5266.
[56] J. W. Heo, A. Banerjee, K. H. Park, Y. S. Jung, S.-T. Hong, *Adv. Energy Mater.* **2018**, *8*, 1702716.
[57] Q. Zhang, C. Zhang, Z. D. Hood, M. Chi, C. Liang, N. H. Jalarvo, M. Yu, H. Wang, *Chem. Mater.* **2020**, *32*, 2264–2271.
[58] D. Zhang, X. Cao, D. Xu, N. Wang, C. Yu, W. Hu, X. Yan, J. Mi, B. Wen, L. Wang, L. Zhang, *Electrochim. Acta* **2018**, *259*, 100–109.
[59] H. Wang, M. Yu, Y. Wang, Z. Feng, Y. Wang, X. Lü, J. Zhu, Y. Ren, C. Liang, *J. Power Sources* **2018**, *401*, 111–116.
[60] S. Xiong, Z. Liu, H. Rong, H. Wang, M. McDaniel, H. Chen, *Sci. Rep.* **2018**, *8*, 9146.
[61] H. Wan, J. P. Mwizerwa, F. Han, W. Weng, J. Yang, C. Wang, X. Yao, *Nano Energy* **2019**, *66*, 104109.
[62] H. Wang, Y. Chen, Z. D. Hood, J. K. Keum, A. S. Pandian, M. Chi, K. An, C. Liang, M. K. Sunkara, *ACS Appl. Energy Mater.* **2018**, *1*, 7028–7034.
[63] T. Kaib, S. Haddadpour, M. Kapitein, P. Bron, C. Schröder, H. Eckert, B. Roling, S. Dehnen, *Chem. Mater.* **2012**, *24*, 2211–2219.
[64] T. Kaib, P. Bron, S. Haddadpour, L. Mayrhofer, L. Pastewka, T. T. Järvi, M. Moseler, B. Roling, S. Dehnen, *Chem. Mater.* **2013**, *25*, 2961–2969.
[65] W. Weng, H. Wan, G. Liu, L. Wu, J. Wu, X. Yao, *ACS Appl. Energy Mater.* **2021**, *4*, 1467–1473.
[66] Deposition Numbers 2172951 (for Na_4SnS_4, **II**), 2172952 (for $Na_{3.99}Sn_{0.99}Sb_{0.01}S_4$, **IIa**), and 2172950 (for $Na_{3.9}Sn_{0.9}Sb_{0.1}S_4$, **IIb**) contain the supplementary crystallographic data for this paper. These data are provided free of charge by the joint Cambridge Crystallographic Data Centre and Fachinformationszentrum Karlsruhe Access Structures service.
[67] M. A. Kraft, L. M. Gronych, T. Famprikis, S. Ohno, W. G. Zeier, *Chem. Mater.* **2020**, *32*, 6566–6576.

[68] W. D. Richards, T. Tsujimura, L. J. Miara, Y. Wang, J. C. Kim, S. P. Ong, I. Uechi, N. Suzuki, G. Ceder, *Nat. Commun.* **2016**, *7*, 11009.
[69] L. Gao, G. Bian, Y. Yang, B. Zhang, X. Wu, K. Wu, *New J. Chem.* **2021**, *45*, 12362–12366.
[70] C. Mundus, G. Taillades, A. Pradel, M. Ribes, *Solid State Nucl. Magn. Reson.* **1996**, *7*, 141–146.
[71] A. Benkada, H. Reinsch, M. Poschmann, J. Krahmer, N. Pienack, W. Bensch, *Inorg. Chem.* **2019**, *58*, 2354–2362.
[72] L. Protesescu, M. Nachtegaal, O. Voznyy, O. Borovinskaya, A. J. Rossini, L. Emsley, C. Copéret, D. Günther, E. H. Sargent, M. V. Kovalenko, *J. Am. Chem. Soc.* **2015**, *137*, 1862–1874.
[73] M. Kaus, H. Stöffler, M. Yavuz, T. Zinkevich, M. Knapp, H. Ehrenberg, S. Indris, *J. Phys. Chem. C* **2017**, *121*, 23370–23376.
[74] J. T. S. Irvine, D. C. Sinclair, A. R. West, *Adv. Mater.* **1990**, *2*, 132–138.
[75] Z. Zhang, P.-N. Roy, H. Li, M. Avdeev, L. F. Nazar, *J. Am. Chem. Soc.* **2019**, *141*, 19360–19372.
[76] S. Xiong, Z. Liu, L. Yang, Y. Ma, W. Xu, J. Bai, H. Chen, *Mater. Today Phys.* **2020**, *15*, 100281.

Manuscript received: February 9, 2022
Accepted manuscript online: June 1, 2022
Version of record online: July 4, 2022

Minor changes have been made to this manuscript since its publication in Early View.